Eur. Phys. J. A **16**, 337–346 (2003)
DOI 10.1140/epja/i2002-10098-4

THE EUROPEAN PHYSICAL JOURNAL A

Spectroscopy of the deformed ^{126}Ce nucleus

C.M. Petrache[1,a], G. Lo Bianco[1], P.G. Bizzeti[2], A.M. Bizzeti-Sona[2], D. Bazzacco[3], S. Lunardi[3], M. Nespolo[3], G. de Angelis[4], D.R. Napoli[4], N. Blasi[5], S. Brant[6], and D. Vretenar[6]

[1] Dipartimento di Fisica, Università di Camerino, and INFN, Sezione di Perugia, Italy
[2] Dipartimento di Fisica and INFN, Sezione di Firenze, Firenze, Italy
[3] Dipartimento di Fisica and INFN, Sezione di Padova, Padova, Italy
[4] INFN, Laboratori Nazionali di Legnaro, Legnaro, Italy
[5] INFN, Sezione di Milano, Milano, Italy
[6] Department of Physics, Faculty of Science, University of Zagreb, 10000 Zagreb, Croatia

Received: 17 July 2002 / Revised version: 7 October 2002 /
Published online: 18 February 2003 –
Communicated by C. Signorini

Abstract. The even-even nucleus ^{126}Ce was studied via in-beam γ-ray spectroscopy using the ^{40}Ca + ^{92}Mo reaction at 190 MeV. Five bands were observed, one of them being identified for the first time. New connecting transitions were identified between the bands, which lead to new spin assignments. The bands are discussed in the framework of the IBM + broken pairs model.

PACS. 23.20.Lv Gamma transitions and level energies – 21.10.Re Collective levels – 21.60.Ev Collective models – 27.60.+j $90 \leq A \leq 149$

1 Introduction

In order to investigate the variation of the level structure in the sequence of Ce nuclei when approaching the proton dripline, we have studied the ^{126}Ce nucleus in an experiment performed with the GASP array [1].

The neighboring even-even Ce nuclei for which spectroscopic information has been published are ^{124}Ce [2] and ^{128}Ce [3]. The ^{126}Ce nucleus was studied recently by Morek *et al.* [4] and Wilson *et al.* [5]. The much higher statistics of the later experiment performed with the GAMMASPHERE array, enabled the extension of the bands observed by Morek *et al.*at much higher spins. However, the lower part of the level scheme, and in particular the connections of the side bands with the ground-state band, was not equally well studied. The same spin-parity assignments for all bands observed previously are maintained in ref. [5], with the exception of band 2, for which a change of parity from positive to negative is proposed. As will result from the present work, the spin-parity assignment for the side bands in ^{126}Ce has to be completely revised. The difficulties encountered in the interpretations of the level scheme under the spin-parity assumptions of the previous papers are completely eliminated with the new spin-parity assignments adopted in the present work. Moreover, the systematics of the side bands in the even-even Ce nuclei shows a smooth variation with neutron number, as expected. In addition to the bands reported previously, we observe one new band consisting of dipole and cross-over quadrupole transitions.

The bands are discussed in the framework of the interacting boson model plus broken pairs.

2 Experimental details

We populated high-spin states in ^{126}Ce using the ^{40}Ca + ^{92}Mo reaction, with a ^{40}Ca beam of 5 pnA intensity and an energy of 190 MeV. The beam was provided by the XTU Tandem accelerator of the Laboratori Nazionali di Legnaro. The target was a self-supporting ^{92}Mo foil with a thickness of 0.5 mg/cm^2. The experimental setup consisted of the GASP array for γ-ray detection and the ISIS silicon ball for charged-particle detection [6].

The GASP array with 40 Compton-suppressed Ge detectors and the 80-element BGO ball was used for a γ^n coincidence measurement. The experimental arrangement in GASP has been carefully prepared, in order to minimize the absorbtion of the low-energy X-rays. Light charged particles (p, d, t and α-particles) were detected with the ISIS ball, which is composed of 40 ΔE-E Si telescopes. Events were written on tape when two or more Ge detectors fired in coincidence with at least two BGO detectors.

[a] e-mail: costel.petrache@unicam.it

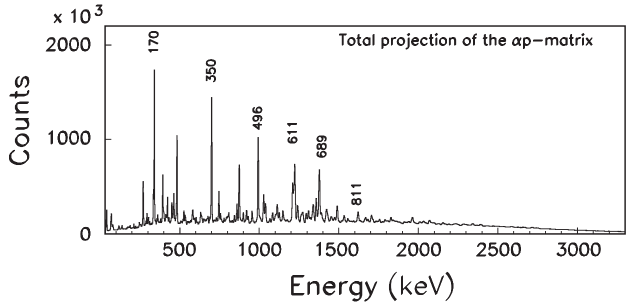

Fig. 1. Total projection of the αp-matrix. Only the most intense transitions of ^{126}Ce are indicated by their energies.

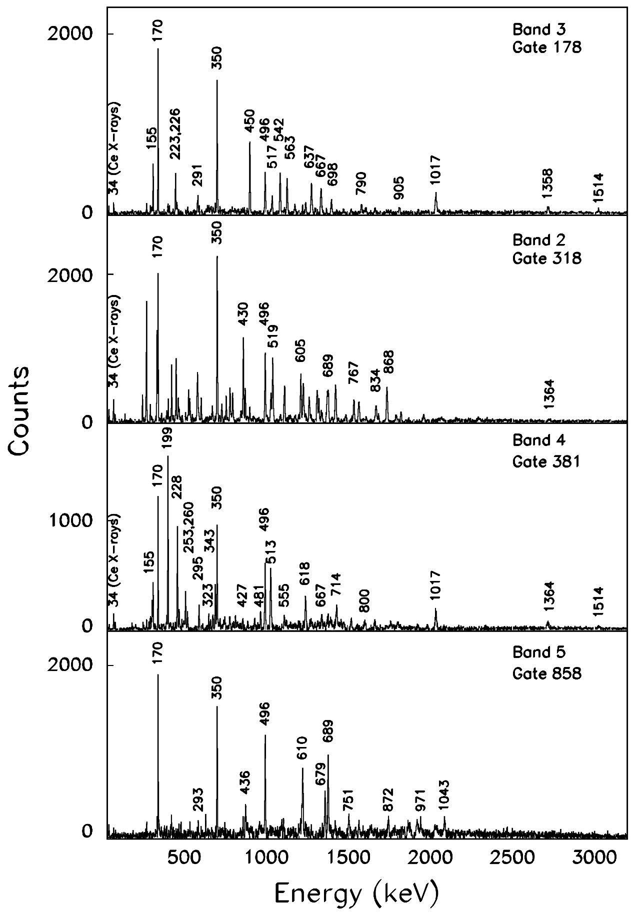

Fig. 2. Coincidence $\gamma\gamma$-spectra obtained from the αp-matrix by gating on clean transitions.

A total of 3.5×10^9 Compton-suppressed events have been collected.

The ^{126}Ce nucleus was populated via the $\alpha 2p$ channel. The charged particles from each event were identified mainly as protons and α-particles and their energy measured. The events were then sorted according to the number of charged-particle detectors that fired in coincidence. For each charged-particle combination E_γ-E_γ and E_γ-E_γ-E_γ matrices were produced off-line for further analysis. The level structure of ^{126}Ce has been derived mainly

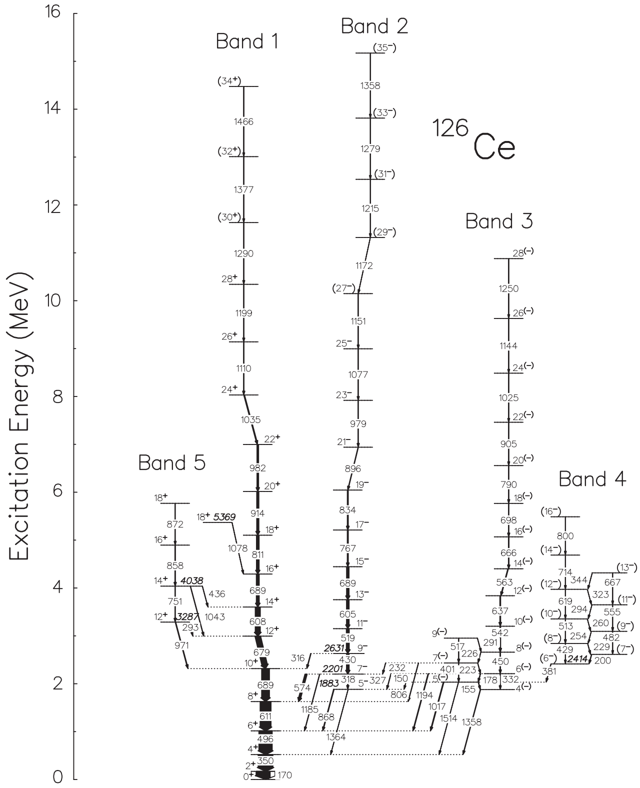

Fig. 3. Level scheme of ^{126}Ce deduced from the present work. The transition intensities are proportional to the width of the arrows.

from the analysis of the αp-gated data, where the statistics was larger and allowed us to observe the weakest transitions. The $\alpha 2p$-gated matrix has been used in a few particular cases requiring very high channel selectivity.

3 Results

The total projection of the αp-matrix is shown in fig. 1. Coincidence spectra showing transitions of bands 2, 3, 4 and 5 of ^{126}Ce are given in fig. 2. They show the new connecting transitions of the side bands with the ground-state band, and are obtained from the αp-matrix by gating on selected clean γ-rays: the 178 keV transition of band 3, the 318 keV transition at the bottom of band 2, the 381 keV transition connecting band 4 to band 3, and the 858 keV transition of band 5.

The decay scheme of ^{126}Ce resulting from the present analysis is shown in fig. 3. Information on the γ-ray transitions is given in table 1. The spins of the new levels have been inferred (when possible) from the combined information obtained from a directional correlation orientation (DCO) analysis as described, *e.g.*, in [7], and from the angular distribution of the γ-rays (see the following section).

Table 1. Gamma-ray energies, intensities and DCO ratios for transitions in ^{126}Ce.

E_γ(keV)^a	Transition intensities^b	DCO ratios^c	Assignment $I_i^\pi \to I_f^\pi$	E_γ(keV)^a	Transition intensities^b	DCO ratios^c	Assignment $I_i^\pi \to I_f^\pi$
149.6	1.1(2)		$5^{(-)} \to 5^{(-)}$	688.6	54(5)	$1.04(4)^q$	$10^+ \to 8^+$
154.6	2.8(2)	$0.65(32)^{sq}$	$5^{(-)} \to 4^{(-)}$	688.6	20(5)	$1.04(4)^q$	$16^+ \to 14^+$
169.7	98(2)	$0.98(2)^q$	$2^+ \to 0^+$	688.9	17(3)	$1.07(9)^q$	$15^{(-)} \to 13^{(-)}$
177.7	3.3(1)	$0.88(23)^{sq}$	$6^{(-)} \to 5^{(-)}$	698.1	4.7(4)	$1.04(13)^{sq}$	$18^{(-)} \to 16^{(-)}$
199.9	3.5(2)		$(7^-) \to (6^-)$	714	2.5(2)		$(14^-) \to (12^-)$
223.3	2.5(2)	$0.68(43)^{sq}$	$7^{(-)} \to 6^{(-)}$	751.4	1.4(2)	$0.96(39)^q$	$14^+ \to 12^+$
226.4	2.2(2)	$0.53(42)^{sq}$	$8^{(-)} \to 7^{(-)}$	766.7	11.7(4)	$1.12(18)^q$	$17^{(-)} \to 15^{(-)}$
228.8	2.5(1)	$0.51(41)^q$	$(8^-) \to (7^-)$	790.2	3.0(2)	$1.01(25)^{sq}$	$20^{(-)} \to 18^{(-)}$
232.3	0.5(1)		$7^{(-)} \to 7^{(-)}$	800	2.0(2)		$(16^-) \to (14^-)$
253.6	1.5(1)		$(9^-) \to (8^-)$	805.9	2(0.5)		$7^{(-)} \to 8^+$
260.0	1.3(1)		$(10^-) \to (9^-)$	810.6	18.3(5)	$1.03(6)^q$	$18^+ \to 16^+$
291.3	2.0(2)		$9^{(-)} \to 8^{(-)}$	834.1	9.1(4)	$0.95(17)^q$	$19^{(-)} \to 17^{(-)}$
292.7	1.3(2)	$0.93(40)^q$	$12^+ \to 12^+$	858.2	3.7(5)	$0.84(17)^q$	$16^+ \to 14^+$
294.5	1.4(3)		$(11^-) \to (10^-)$	867.5	3.7(3)	$0.75(21)^{sq}$	$5^{(-)} \to 6^+$
315.7	3.5(3)	$0.71(20)^{sq}$	$9^{(-)} \to 10^+$	871.8	1.3(4)	$0.97(20)^q$	$18^+ \to 16^+$
317.9	3.5(3)	$0.92(20)^q$	$7^{(-)} \to 5^{(-)}$	895.6	5.9(4)	$1.07(15)^{sq}$	$21^{(-)} \to 19^{(-)}$
323	1.9(1)		$(12^-) \to (11^-)$	905.4	2.8(2)	$1.05(21)^{sq}$	$22^{(-)} \to 20^{(-)}$
326.7	2.0(1)	$0.62(21)^q$	$6^{(-)} \to 5^{(-)}$	914.2	14.9(4)	$1.04(12)^{sq}$	$20^+ \to 18^+$
331.9	2.9(2)	$1.14(50)^q$	$6^{(-)} \to 4^{(-)}$	971.4	2.4(2)	$0.91(24)^q$	$12^+ \to 10^+$
344	2.7(3)		$(13^-) \to (12^-)$	978.5	3.8(3)	$1.20(25)^{sq}$	$23^{(-)} \to 21^{(-)}$
349.8	100(2)	$1.04(2)^q$	$4^+ \to 2^+$	981.6	11.2(5)	$1.01(12)^{sq}$	$22^+ \to 20^+$
381.0	2.3(2)	$1.42(16)^{d,e}$	$(6^-) \to 5^{(-)}$	1016.7	7.6(2)	$0.54(9)^{sq}$	$5^{(-)} \to 6^+$
400.6	3.1(2)	$1.87(85)^d$	$7^{(-)} \to 5^{(-)}$	1025.1	1.6(2)		$(24^-) \to 22^{(-)}$
428.6	< 0.5		$(8^-) \to (6^-)$	1035.2	6.2(6)	$1.05(16)^{sq}$	$24^+ \to 22^+$
429.7	20.1(4)	$0.97(18)^q$	$9^{(-)} \to 7^{(-)}$	1043.1	2.6(2)		$14^+ \to 12^+$
436.4	1.4(2)		$14^+ \to 14^+$	1076.8	2.6(2)	$1.00(24)^{sq}$	$25^{(-)} \to 23^{(-)}$
449.5	6.6(4)	$1.09(32)^q$	$8^{(-)} \to 6^{(-)}$	1079	1.2(5)	$1.07(49)^q$	$18^+ \to 16^+$
482.5	1.1(1)		$(9^-) \to (7^-)$	1110.4	3.2(2)	$1.01(23)^{sq}$	$26^+ \to 24^+$
496.3	92(1)	$1.04(2)^q$	$6^+ \to 4^+$	1142.4	1.0(2)		$(26^-) \to (24^-)$
513.1	3.5(3)		$(10^-) \to (8^-)$	1151.4	1.8(2)		$(27^-) \to (25^-)$
517.1	4.6(2)	$1.10(38)^q$	$9^{(-)} \to 7^{(-)}$	1172.1	1.2(2)		$(29^-) \to (27^-)$
519.4	21(1)	$1.03(16)^q$	$11^{(-)} \to 9^{(-)}$	1185.2	2.1(5)	$0.53(20)^{sq}$	$7^{(-)} \to 6^+$
541.9	6.8(1.5)	$1.0(2)^{sq}$	$10^{(-)} \to 8^{(-)}$	1194.3	6.3(3)	$1.06(18)^q$	$6^{(-)} \to 6^+$
554.8	2.3(1)		$(11^-) \to (9^-)$	1199.2	1.7(9)	$1.01(40)^{sq}$	$28^+ \to 26^+$
563.2	6.1(3)	$1.01(10)^{sq}$	$14^{(-)} \to 12^{(-)}$	1214.5	1.1(2)		$(31^-) \to (29^-)$
573.9	15.2(5)	$0.68(4)^{sq}$	$7^{(-)} \to 8^+$	1251.3	0.4(1)		$(28^-) \to (26^-)$
604.8	17.8(8)	$1.15(9)^q$	$13^{(-)} \to 11^{(-)}$	1279.0	< 0.5		$(33^-) \to (31^-)$
607.9	35(1)	$1.04(9)^q$	$14^+ \to 12^+$	1290	1(0.2)		$(30^+) \to (28^+)$
611.2	75(2)	$0.95(4)^q$	$8^+ \to 6^+$	1358.3	< 0.1		$(35^-) \to (33^-)$
619.1	4.5(4)		$(12^-) \to (10^-)$	1358.4	5.3(4)	$0.81(22)^{sq}$	$4^{(-)} \to 4^+$
637.2	7.8(5)	$1.03(10)^{sq}$	$12^{(-)} \to 10^{(-)}$	1364	0.5(3)		$5^{(-)} \to 4^+$
666.4	5.3(3)	$1.06(13)^{sq}$	$16^{(-)} \to 14^{(-)}$	1377.4	0.5(2)		$(32^+) \to (30^+)$
667	< 0.5		$(13^-) \to (11^-)$	1464.7	0.3(1)		$(34^+) \to (32^+)$
678.7	39(2)	$0.99(5)^q$	$12^+ \to 10^+$	1514	< 0.1	$0.60(20)^{sq}$	$5^{(-)} \to 4^+$

^{a} The error on the transition energies is 0.2 keV for transitions below 1000 keV and intensities larger than 5% of the ^{126}Ce channel, 0.5 keV for transitions above 1000 keV and intensities lower than 5%, and 1 keV for transitions above 1200 keV and/or weaker than 1%.

^{b} Relative intensities corrected for efficiency. The transition intensities were obtained from a combination of total projection and gated spectra.

^{c} The DCO ratios have been deduced from an asymmetric $\gamma\gamma$ coincidence matrix gated by the αp combination of charged particles detected by the isotropic ISIS ball. The tentative spin-parity of the states are given in parenthesis.

^{d} Gated by a "stretched" dipole transition.

^{e} See also the discussion in the text of other DCO ratios related to the 381 keV transition.

^{q} Gated by a "stretched" quadrupole transition.

^{sq} Gated by a sum "stretched" quadrupole transition.

3.1 Band properties and spin assignment

3.1.1 Band 1

We confirm all the γ-rays up to spin (34^+) that were assigned in ref. [5] to band 1. The transition energies and intensities are in general good agreement with the previously reported values, with only three exceptions: the energies of the $24^+ \to 22^+$ and $32^+ \to 30^+$ transitions (1035.2 and 1377.4 keV) are larger by 0.8 and 2.4 keV, respectively, and the intensity of the 170 keV $2^+ \to 0^+$ is larger by 25%.

3.1.2 Band 2

We observe band 2 up to spin (35^-). There are some differences with respect to data previously reported in ref. [5]. The first one is that, due to the different reaction used in our experiment ($^{40}\mathrm{Ca} + {}^{92}\mathrm{Mo}$), which employed a lighter projectile than in ref. [5] ($^{64}\mathrm{Zn} + {}^{64}\mathrm{Zn}$), the total angular momentum of the compound nucleus was probably lower and we could not see the top-most 1442 keV transition reported in ref. [5]. The other differences are: the energies of the $(31^-) \to (29^-)$ and $(35^-) \to (33^-)$ transitions (1214.5 and 1358.3 keV) are larger by 1.5 and 3 keV, respectively, whereas the energies of the $17^- \to 15^-$ and $27^- \to 25^-$ transitions (766.7 and 1151.4 keV) are larger by about 1 keV; the intensities of the 896, 1077, 1151, 1172 and 1185 keV transitions are larger by a factor 1.5–2 than those reported in ref. [5]; we observed a new $5^- \to 4^+$, 1364 keV transition at the bottom of the band.

The most important difference with respect to ref. [5] comes from the spin assignment: to the lowest level of band 2 is assigned spin and parity $5^{(-)}$ —which turns out to be in agreement with the systematics of this region of nuclei— while in ref. [5] the authors assing spin-parity (7^-) to the same state. The difference in spin assignment has important consequences regarding the configuration of the band and the properties of the connecting transitions with states of band 1.

The values of DCO ratios measured in the present work are usually in agreement with those reported in ref. [5] (see table 1), with one important exception: that of the 1185 keV transition (from band 2 to band 1), in coincidence with the stretched $E2$ transitions of band 2 populating the $E_x = 2201$ keV level. For this case, a value of 1.6 ± 0.3 is reported in ref. [5], while in our experiment it turns out to be 0.53 ± 0.20, *i.e.* a factor of three lower. The reason of the discrepancy is not clear. Apparently, our value would be hardly consistent with the value ≈ 1 expected for a stretched quadrupole transition and, *a fortiori*, with the stretched $E3$ character proposed in ref. [5]. In fact, in the latter case, the DCO ratio would be larger than 1 and would approach 1.2 for almost complete alignment. Instead, we observe a value which is typical of stretched dipole transitions.

On this basis, we are forced to assign an angular momentum $J = 5$ to the lowest level of band 2 and, as a consequence, to decrease by two units the angular momenta of all the higher states of this band. Values of DCO ratios for other γ transitions which were consistent with the spin assignments of ref. [5], remain also consistent with the present ones. In fact, the DCO ratios of pure dipole transitions with $J-1 \to J$ are very similar to those for $J \to J-1$ (0.65 and 0.61, respectively, for alignment $\sigma/J = 0.25$ and in coincidence with a stretched quadrupole transition).

In view of the crucial role of the DCO ratios involving the 1185 keV transition, several independent checks have been performed. Namely, other DCO ratios have been evaluated, with the following results (in parenthesis, the energy of the transition in coincidence with the 1185 keV one): 0.50 ± 0.21 (430 keV), 0.53 ± 0.28 (519 keV), 0.58 ± 0.14 (430 + 519 keV), 0.44 ± 0.11 (430 + 519 + 767 keV), 0.52 ± 0.11 (430 + 519 + 767 + 834 keV), 0.78 ± 0.25 (170 keV), 0.67 ± 0.37 (350 keV), 0.70 ± 0.23 (496 keV). Although the experimental errors are admittedly large for most of the above results, this body of results apparently confirms our conclusion, at variance with that of ref. [5].

The value $J = 5$ for the spin of the lowest level of band 2, proposed on the basis of DCO ratios, is also supported by the population pattern of the observed bands in ^{126}Ce. In fact, the intensity of the various bands decreases with the excitation energy above yrast: the intensity of band 2 is intermediate between that of band 1 and 3 (see table 1 and fig. 3). In general, with the adopted spin values for the different bands observed in ^{126}Ce which are discussed in this and the following subsections, the intensity of the bands at spin $18\hbar$ decreases with increasing excitation energy from 18% for band 1, to 9% for band 2, to 5% for band 3, to 1% for band 5 and to $< 1\%$ for band 4.

When we try to assign a definite parity to band 2, one realizes that the measured DCO ratios for the connecting transitions to band 1 are compatible with either $E1$ or $M1/E2$ transitions. We prefere to assign negative parity to band 2 on the basis of the following considerations: i) the DCO ratio of the 1185 keV transition is 0.53(20), being compatible with an $E1$ character; ii) the systematics of the negative-parity bands in the even-even neighboring nuclei; iii) the low-spin two-quasiparticle configurations close to the yrast line are predicted to have negative parity.

The spin-parity assignment to band 2 resolves the problem of the enormous $B(E3)$ value (several thousands of W.u.) that would result for the 1185 keV transition if it were of $E3$ character as assigned in ref. [5].

3.1.3 Band 3

We confirm all transitions previously assigned to band 3 in ref. [5], and add ten new transitions: five transitions with energy 223, 226, 291, 401 and 517 keV which are positioned above the 155 keV transition [5], two transitions with energies of 806 and 1514 keV which connect states of band 3 to band 1, and three transitions of 150, 232 and 327 keV which connect states of band 3 to band 2. The new observed transitions show that band 3 is of semi-decoupled character, with in-band dipole and cross-over quadrupole transitions.

There is a significant difference between our data and those reported in ref. [5]: we find transition intensities that are larger by a factor of two with respect to the intensities of these transitions given in ref. [5]. This can be due to the different population of the side bands in the two reactions. Another difference is related to the energies of the 563.2, 790.2 and 1251.3 keV transitions, which are larger by 1.1, 0.8 and 2.3 keV, respectively, than the values reported in ref. [5].

The spin assignment to band 3 is mainly based on the DCO ratios of the 1017, 1194 and 1358 keV transitions towards band 1. The measured DCO ratio $R_{\rm DCO} = 0.54(9)$ for the 1017 keV transition, the strongest among the out-of-band transitions, indicates a $\Delta I = 1$ transition, being compatible with either $E1$ or mixed $M1/E2$ transition with a small $E2$ component. The possible spins of the level de-excited by the 1017 keV transition are 5, 6 or 7. The spin-7 value can be excluded, since in that case the observed 1514 keV transition from the $E_x = 2033$ keV level would be an unexpected $\Delta I = 3$ transition. The spin-6 alternative would force us to assign positive parity to band 3, since only then one can account for the large DCO ratios of the 1194 and 1358 keV transitions, which would be of $M1/E2$ character. But in this case the 327 keV transition would be of stretched $E2$ character, which is not in agreement with the measured DCO ratio of 0.62(21), which indicates a $\Delta I = 1$ mixed $M1/E2$ character. A negative-parity assignment in the spin-6 alternative, would lead to an $E1/M2$ character for the 1194 and 1358 keV transitions, and the large DCO ratios of these transitions would imply large $M2$ admixtures, which are unexpected in this mass region.

We prefer the spin-5 value for the state de-excited by the 1017 keV transition. In this case the 1017 keV transition is a stretched transition in agreement with the measured DCO ratio of 0.54(9), the DCO ratios of the 1194 and 1358 keV transitions of 1.06(18) and 0.81(22), respectively, fit well with the expected values for unstretched dipole ($\Delta J = 0$) transitions (DCO ratio close to 1), and the DCO ratio of the 327 keV transition of 0.62(21) is in agreement with a $\Delta I = 1$ transition. The other two connecting transitions of 806 and 1514 keV become in this scenario $J - 1 \rightarrow J$ and $J \rightarrow J - 1$ transitions, respectively, of stretched dipole character. Therefore, we assign spin 5 to the $E_x = 2033$ keV level of band 3.

No strong arguments for the parity assignment to band 3 are provided by the present experimental results. However, several concording (although individually weak) indications favour the assignment of negative parity which is favoured by the systematics, as —in this region of nuclei— the decay out of a band strongly prefers states with the same parity, if available. In fact, dipole transitions from levels of band 3 to those of band 2 (of negative parity) are strongly favoured with respect to dipole transitions to band 1 (positive parity) and, according to the systematics, it is very probable that the former are $M1$ and the latter $E1$. Moreover, no indication of $E2$ transitions from the lowest level of band 3 to those of band 1 has been found, while several transitions of this kind exist between levels of band 5 and of band 1.

3.1.4 Band 4

Band 4 was not observed previously, even if the 200, 229, 381, 513 and 619 keV transitions were reported in ref. [5] and observed in coincidence with band 3. We have been able to identify several new transitions having coincidence relationships with the above-mentioned transitions and organize them in the form of a semi-decoupled band, with dipole and cross-over quadrupole transitions. As is the case for band 3, the intensities that we find for the transitions reported previously in ref. [5] are larger by a factor of two. This band is linked to the other observed levels in ^{126}Ce by only one transition of 381 keV. The spin of the band head could be 5, 6 or 7, due to the 381 keV decay to the $J = 5$ level of band 3. The value $J = 6$ is preferred, due to the the fact that DCO ratios between the 381 keV transition and several $\Delta J = 1$ and $\Delta J = 2$ transitions are consistent with a mixed dipole + quadrupole assignment, while it is only marginally compatible with a stretched quadrupole. In fact the DCO ratios obtained by gating on the 381 keV transition for the 170 and 350 keV transitions of the ground-state band are 1.46(36) and 1.18(28) respectively, whereas those of the 200 and 229 keV dipole transitions of band 4 are 0.79(9) and 0.87(15), respectively. The DCO ratio of the 200 keV transition of band 4 gating on the sum of the 170 and 350 keV transitions of the ground-state band is 0.56(10), suggesting pure dipole character for the 200 keV transition. Finally, the DCO ratio of the 381 keV transition obtained by gating on the 200 keV pure dipole transition is 1.42(16), which suggests that the 381 keV transition has a mixed $M1/E2$ character. Spin and parity assignments to the levels of this band must, however, only be considered as temptative.

3.1.5 Band 5

We confirm the transitions previously reported in ref. [5] only up to spin 16^+. Above the 858.2 keV transition (whose energy is larger by 1.5 keV with respect to that reported in ref. [5]), we place the new 872 keV transition. In addition to the previously reported connecting transitions with energies of 971 and 1043 keV, we found two other transitions of 293 and 436 keV. The transitions linking the observed band 5 to levels of band 1 are weak and the errors on their DCO ratios are quite large. However, the extracted DCO values are close to $R_{\rm DCO} = 1$, indicating either stretched $E2$ or $\Delta I = 0$ mixed $M1/E2$ transitions. The presence of transitions from, *e.g.*, the lowest observed level of band 5 to both the 10^+ and 12^+ levels of band 1, strongly suggests a 12^+ spin value for that level, since the alternative 10^+ spin would lead to an unexpected up-hill $10^+ \rightarrow 12^+$ 293 keV transition.

With the present spin-parity assignments to the side bands observed in ^{126}Ce we find a nice agreement with

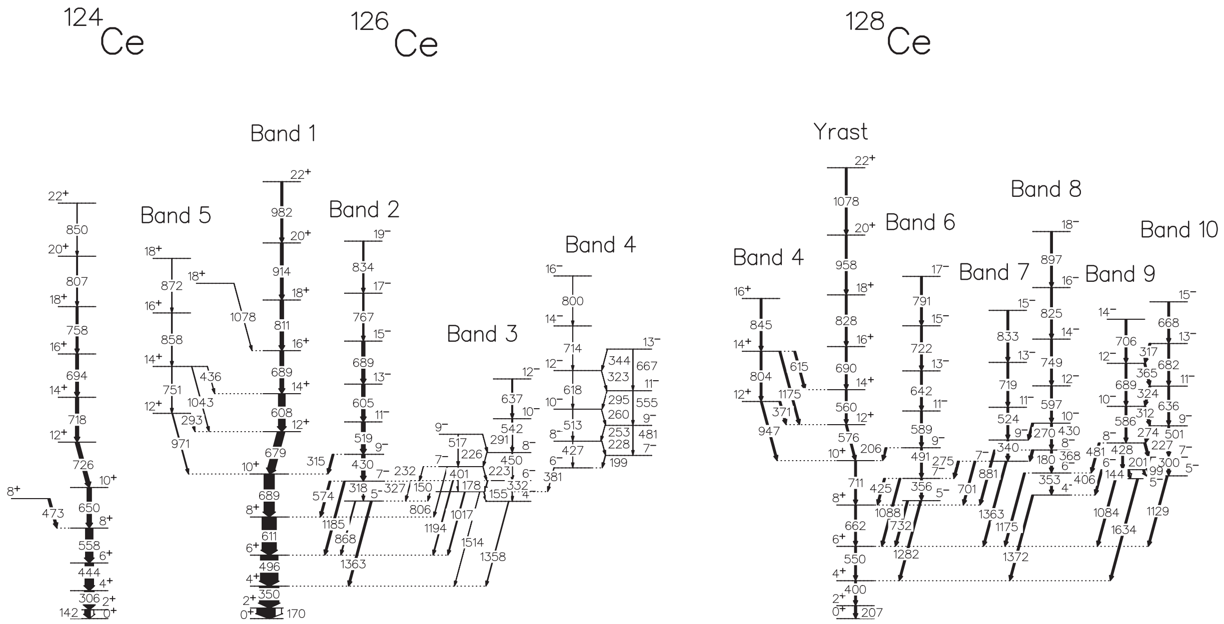

Fig. 4. Low-lying level schemes of ^{124}Ce, ^{126}Ce and ^{128}Ce. The bands of ^{128}Ce are labelled as in ref. [3].

the corresponding bands observed in the neighboring even-even Ce nuclei. For comparison, the low-lying level scheme of ^{126}Ce and its neighbours ^{124}Ce and ^{128}Ce are shown in the same drawing in fig. 4 [2,3]. One can observe that the counterpart of band 2 in ^{126}Ce is band 6 in ^{128}Ce. The decay pattern of band 2 in ^{126}Ce and band 6 in ^{128}Ce [3] (called band 7 in ref. [8]) is very similar, consisting of $J-1 \to J$ transitions that are stronger than the $J \to J-1$ transitions. One also finds similarities between the dipole bands 3 and 4 of ^{126}Ce and the dipole bands drawn on the right side of the level scheme of ^{128}Ce. In particular, band 3 of ^{126}Ce decays towards bands 1 and 2, as is the case for bands 7 and 8 of ^{128}Ce [8], which would therefore correspond to band 3 of ^{126}Ce. The counterpart of band 4 in ^{126}Ce is formed by a pair of bands 9 and 10 in ^{128}Ce. Band 5 in ^{126}Ce is also observed in ^{128}Ce, where is called band 4. The decay pattern from these two bands towards the yrast band is identical in the two nuclei, indicating their similar configuration.

3.2 Interacting boson plus broken pairs model analysis of the level structure of ^{126}Ce

The structure of positive- and negative-parity bands in ^{126}Ce is analyzed in the framework of the Interacting Boson plus Broken Pairs Model (IBBPM) [9–12]. Based on the interacting-boson approximation (IBA) [13,14], the model describes the structure of high-spin states in the region $10\hbar \leq I \leq 30\hbar$. The collective model space is that of the IBM-1 model [14]: the boson space consists of s and d bosons, with no distinction between protons and neutrons. High-spin states are generated not only by the alignment of d-bosons, but also by coupling fermion pairs to the boson core. A boson can be destroyed, *i.e.* a correlated fermion pair can be broken, by the Coriolis interaction and the resulting non-collective fermion pair recouples to the core. High-spin states are described in terms of broken pairs. The IBM plus broken pairs model is especially relevant for transitional regions, where single-particle excitations and vibrational collectivity are dominant modes, and the traditional cranking approach to high-spin physics is not adequate. Another advantage of the IBM plus broken pairs calculations is that they are performed in the laboratory system, and the resulting excitation energies and electromagnetic properties can be directly compared with experimental data. This framework has been very successfully applied in the analysis of high-spin structures in the Hg, Sr-Zr, Cd and Nd-Sm regions.

The model Hamiltonian contains four basic terms: the IBM-1 boson Hamiltonian [14], the fermion Hamiltonian, the boson-fermion interactions of IBFM-1 [15], and a pair breaking interaction that mixes states with different number of fermions [9]. ^{126}Ce lies in the transitional region between deformed nuclei (lighter Ce isotopes) described by the $SU(3)$ limit of the IBM, and γ-soft nuclei (heavier Ce isotopes) which correspond to the $O(6)$ limit of the IBM. The $SU(3)$-$O(6)$ transition can be described by the boson Hamiltonian

$$H_{\mathrm{IBM}} = -\frac{\alpha}{10}\, Q \cdot Q \, + \, \frac{\beta}{10}\, L \cdot L \,, \tag{1}$$

and is determined by the value of the parameter χ in the quadrupole boson operator [14]. The limiting cases are: $\chi = 0$ which corresponds to the $O(6)$ limit of the IBM-1, and $\chi = -\frac{\sqrt{7}}{2}$ which describes a prolate shape in the $SU(3)$ dynamical symmetry limit. The parameters for ^{126}Ce are adjusted to the experimental collective states of angular momentum $I \leq 10$ (bands 1 and 6): $\alpha = 0.19$ MeV, $\beta = 0.16$ MeV, $\chi = -0.85$, with the boson number $N = 11$. The values of the boson parameters are very close to those of ^{124}Ce, which was used as the boson

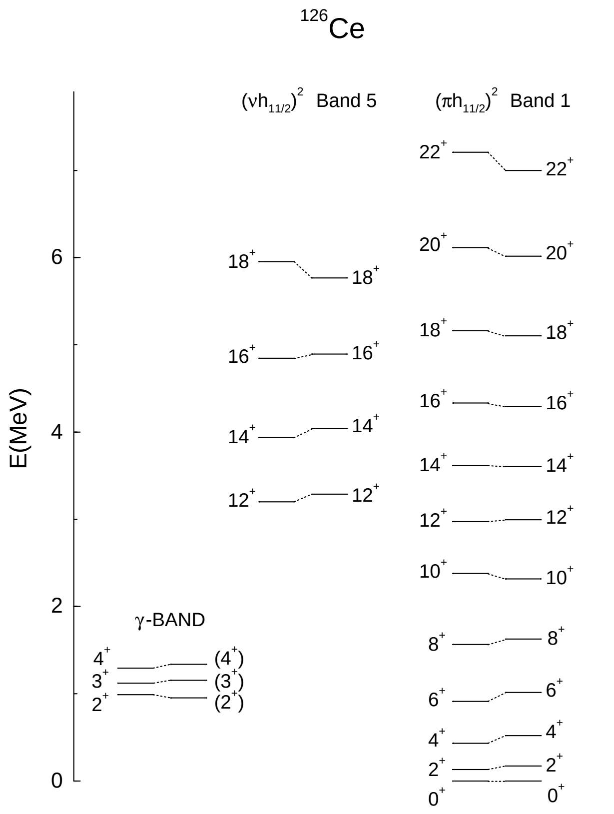

Fig. 5. Positive-parity states in ^{126}Ce compared with the results of the Interacting Boson plus Broken Pairs Model calculation. The levels of the γ-band were taken from ref. [16].

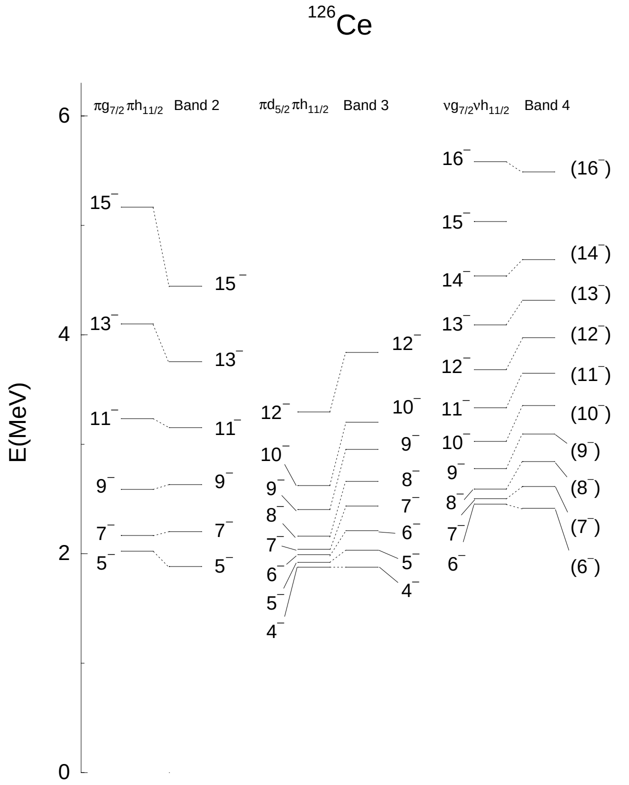

Fig. 6. Bands of negative-parity states in ^{126}Ce compared with the results of the IBBPM calculation.

core of the odd-odd nucleus ^{126}Pr in a recent calculation of ref. [17]. The value $\chi = -0.85$ is consistently used in the boson operator of the fermion-boson quadrupole interaction (both for protons and neutrons), as well as in the $E2$ boson operator.

The calculated proton quasiparticle energies ε and occupation probabilities v^2 have the following values: $\varepsilon(\pi g_{7/2}) = 1.01$ MeV, $\varepsilon(\pi d_{5/2}) = 1.03$ MeV, $\varepsilon(\pi h_{11/2}) = 1.70$ MeV, $v^2(\pi g_{7/2}) = 0.63$, $v^2(\pi d_{5/2}) = 0.35$, $v^2(\pi h_{11/2}) = 0.06$. They result from a BCS calculation with Kisslinger-Sorensen single-particle energies [18], and $G = \frac{23}{A}$ MeV for the strength of the pairing interaction. The only exception is the quasiparticle energy of $\pi h_{11/2}$, which is reduced by 0.3 MeV with respect to the BCS calculation. This modification is required by the experimental position of the 12_1^+ state.

The parameterization of neutron particle energies for ^{126}Pr in ref. [17] was based on data from ref. [19]. In the present analysis an improved parameterization, based on new experimental data on ^{125}Ce [20], is used for the neutron particle energies E: $E(d_{5/2}) = 0$ MeV, $E(g_{7/2}) = 0.05$ MeV, $E(h_{11/2}) = 1.15$ MeV, $E(s_{1/2}) = 1.55$ MeV and $E(d_{3/2}) = 1.9$ MeV. In a BCS calculation with $G = \frac{23}{A}$ MeV for the strength of the pairing interaction, the following values of neutron quasiparticle energies and occupation probabilities are obtained: $\varepsilon(\nu h_{11/2}) = 1.28$ MeV, $\varepsilon(\nu s_{1/2}) = 1.40$ MeV, $\varepsilon(\nu d_{3/2}) = 1.57$ MeV, $\varepsilon(\nu g_{7/2}) = 1.60$ MeV, $\varepsilon(\nu d_{5/2}) = 1.63$ MeV, $\varepsilon(\nu f_{7/2}) = 5.28$ MeV, $v^2(\nu h_{11/2}) = 0.43$, $v^2(\nu s_{1/2}) = 0.30$, $v^2(\nu d_{3/2}) = 0.21$, $v^2(\nu g_{7/2}) = 0.80$, $v^2(\nu d_{5/2}) = 0.81$ and $v^2(\nu f_{7/2}) = 0.01$. A discussion on the role of the $\nu f_{7/2}$ orbital in the high-spin structure of this mass region can be found in ref. [17].

The strength parameters of the boson-fermion interaction [15] are (all values in MeV): $A_0^\pi = 0.065$, $\Gamma_0^\pi = 0.25$, $\Lambda_0^\pi = 11.0$, $A_0^\nu = 0.04$, $\Gamma_0^\nu = 0.5$, $\Lambda_0^\nu = 1.6$ for states of positive parity, and $A_0^\pi = -0.05$, $\Gamma_0^\pi = 0.4$, $\Lambda_0^\pi = 4.0$, $A_0^\nu = 0.04$, $\Gamma_0^\nu = 0.2$, $\Lambda_0^\nu = 1.0$ for states of negative parity. The proton fermion-boson interaction strengths for states of positive parity are basically those used for ^{125,126}Pr [17], with the exception of the strength of the exchange interaction, which is considerably larger than in ref. [17]. This parameterization is also used in the calculation of ^{124}Ce [20]. For negative-parity states, the interaction strengths of the dynamical and exchange proton fermion-boson interactions are similar to those used for odd-A Pr nuclei in ref. [17]. In the analysis of ref. [17] very limited information on the level spectrum of ^{125}Ce was used to determine the neutron fermion-boson interaction strengths. Based on new experimental data on ^{125}Ce, these parameters have been determined much more accurately in ref. [20]. Their values, used in the description of low- and high-spin states in ^{125}Ce, are very similar to the ones used in the present analysis.

The boson operator of the dynamical proton fermion-boson interaction contains the additional term

$$\eta^{\pi} \sum_{L_1 L_2} \left[\left(d^{\dagger} \times \tilde{d} \right)^{(L_1)} \left(d^{\dagger} \times \tilde{d} \right)^{(L_2)} \right]^{(2)} ,$$

introduced in ref. [21]. In the present calculation, $\eta^{\pi} = 0.3$ for positive-parity states and $\eta^{\pi} = -0.3$ for negative-parity states. The strength parameter of the pair-breaking interaction is $U_2 = 0.25$ MeV, both for proton pairs and neutron pairs.

In figs. 5 and 6 the calculated spectrum of positive- and negative-parity states is compared with the experimental bands of ^{126}Ce. The calculation is performed in a configuration space of boson states, with either one broken proton pair or one broken neutron pair. Only a few lowest calculated states of each angular momentum, *i.e.* those which have a possible experimental counterpart, are shown in figs. 5 and 6. For $I \leq 10^+$ the experimental yrast sequence 1 corresponds to the collective $SU(3)$-$O(6)$ ground-state band. Between $I = 10^+$ and $I = 12^+$ a band based on the $(\pi h_{11/2})^2$ configuration enters the yrast line. For $12^+ \leq I < 24^+$ the yrast states are based on the two-proton configuration $(\pi h_{11/2})^2$ coupled to the ground-state band of the boson core. Yrast states with $I \geq 24^+$ are probably based on a four-proton configuration. In the present analysis we did not calculate states based on two broken pairs. Our description of the structure of the experimental sequence 1 is in accordance with the systematics of high-spin structures in this mass region, and also with the predictions of the cranking model [4].

The experimental sequence 5 corresponds to the lowest band based on the $(\nu h_{11/2})^2$ configuration. The forking of the ground-state band into two S-bands, one proton and one neutron, is a common feature in light Ce, Ba and Xe nuclei [22]. The present calculation, performed in the laboratory frame, agrees with the description of the forking mechanism in the cranking framework [22].

The triplet of experimental states (band 6) corresponds to the collective γ-band.

From the calculated proton single-quasiparticle energies it is evident that the lowest negative-parity two-proton bands will be based on the $(\pi g_{7/2}\ \pi h_{11/2})$ and $(\pi d_{5/2}\ \pi h_{11/2})$ configurations. The structure of the wave functions of the two-neutron negative-parity bands is more complicated. All neutron valence shell orbitals are active and a pronounced fragmentation of the wave functions can be expected [20]. However, from the comparison of the calculated and experimental excitation energies and transition intensities, it results that the main configuration of the experimental band 2 is $(\pi g_{7/2}\ \pi h_{11/2})$, and that of the experimental band 4 is $(\nu g_{7/2}\ \nu h_{11/2})$. The other branch of the $(\pi g_{7/2}\ \pi h_{11/2})$ configuration with opposite signature is calculated close above band 2, but the transitions between the two branches are weak, and this is probably the reason why the second branch has not been observed in experiment. We also tentatively assign the configuration $(\pi d_{5/2}\ \pi h_{11/2})$ to the experimental band 3, although the calculated moment of inertia is much higher. We notice that in all three negative-parity sequences the calculated energy differences in the low-spin region are considerably smaller than the corresponding experimental values. This is due to the strong mixing of the zero- and one-boson components in the wave functions, and could not be improved in the present calculation.

The transition probabilities are calculated with the following set of effective charges and gyromagnetic ratios [17]: $e^{\pi} = 1.0$, $e^{\nu} = 0.5$, $e^{\mathrm{vib}} = 0.95$, $g_l^{\pi} = 1.0$, $g_s^{\pi} = 0.5\, g_s^{\pi,\mathrm{free}} = 2.793$, $g_l^{\nu} = 0$, $g_s^{\nu} = 0.5\, g_s^{\nu,\mathrm{free}} = -1.913$, $g_R = \frac{Z}{A} = 0.460$. In table 2 we include the calculated $B(E2)$ and $B(M1)$ values for the transitions observed in experiment, and compare the transition intensities with the experimental values. A very good agreement is found between theory and experiment for all intraband transitions, except possibly for band 3. For interband transitions we notice that the transitions from the 12^+ and 14^+ states of the band 5 into states of band 1 are underestimated in the calculation. This is due to the fact that the model Hamiltonian does not contain terms which mix two-proton with two-neutron configurations. The band heads of the $(\pi h_{11/2})^2$ and $(\nu h_{11/2})^2$ bands are states with angular momentum 10^+, not seen in experiment. The calculation predicts weak transitions (due to the small transition energies) from the 12^+ states into the corresponding 10^+ states, but still above the experimental limit. However, a strong mixing between the $(\pi h_{11/2})^2$ and $(\nu h_{11/2})^2$ configurations would reduce these transitions even more, and this could explain why the 10^+ states have not been observed.

The next even-even isotope ^{128}Ce, although softer than ^{126}Ce, displays an almost identical band structure. Therefore, on the basis of the present calculation for ^{126}Ce, we can assign the following configurations to the bands observed in ^{128}Ce (fig. 3): the yrast sequence corresponds to the collective $SU(3)$-$O(6)$ ground-state band for $I \leq 10^+$ and to $(\pi h_{11/2})^2$ for $I \geq 12^+$, band 4 has the structure $(\nu h_{11/2})^2$ coupled to the ground-state band of the boson core, $(\pi g_{7/2}\ \pi h_{11/2})$ for band 6, $(\pi d_{5/2}\ \pi h_{11/2})$ for bands 7 and 8, and finally $(\nu g_{7/2}\ \nu h_{11/2})$ for bands 9 and 10.

4 Conclusions

The level scheme of the nucleus ^{126}Ce has been studied in detail. New spins were assigned to band 2, which resolve the problem related to an unrealistic high $B(E3)$ strength reported previously for a connecting transitions between band 2 and the ground-state band. New connecting transitions were identified and a new band was discovered. The observed level structures have been discussed in the framework of the IBM plus broken pairs model. Good agreement between theory and experiment was obtained for the positive-parity states up to spin 22. The agreement is not so good for the energies of the negative-parity states. This can be due to the mixing of the zero- and one-boson components in the wave functions, which is not included in the present calculations.

Table 2. Electromagnetic transition properties of states in ^{126}Ce. In the first column the transition is denoted by its initial and final angular-momentum and parity assignments I_k^π. The index k is the label of the band. In the third and fourth columns the calculated $B(E2)$ and $B(M1)$ values are shown, respectively. The experimental and IBBPM γ-intensities are compared in the last two columns. Only those transitions with calculated intensity > 0.01 % of the main branch are included.

Transition		IBBPM		Branchings	
$J_i^\pi \to J_f^\pi$	E_γ (keV)	$B(E2)$ (e^2b^2)	$B(M1)$ (μ_N^2)	Exp (%)	IBBPM (%)
$2_1^+ \to 0_1^+$	170	0.3007		100	100
$4_1^+ \to 2_1^+$	350	0.4216		100	100
$6_1^+ \to 4_1^+$	496	0.4486		100	100
$8_1^+ \to 6_1^+$	611	0.4450		100	100
$10_1^+ \to 8_1^+$	689	0.3734		100	100
$12_1^+ \to 10_1^+$	679	0.0861		100	100
$14_1^+ \to 12_1^+$	608	0.3391		100	100
$16_1^+ \to 14_1^+$	689	0.3373		100	100
$18_1^+ \to 16_1^+$	811	0.3362		100	100
$20_1^+ \to 18_1^+$	914	0.3251		100	100
$22_1^+ \to 20_1^+$	982	0.3023		100	100
$12_5^+ \to 12_1^+$	293	0.0000	0.0080	35	1
$\to 10_1^+$	971	0.0306		65	99
$14_5^+ \to 14_1^+$	436	0.0000	0.0002	26	0.03
$\to 12_5^+$	751	0.3804		26	99.9
$\to 12_1^+$	1043	0.0001		48	0.1
$16_5^+ \to 14_5^+$	858	0.3880		100	100
$\to 14_1^+$		0.00003			0.06
$18_5^+ \to 16_5^+$	872	0.3747		100	100
$2_6^+ \to 4_1^+$		0.0003			0.2
$\to 2_1^+$	785	0.0035	0.0000	62	36
$\to 0_1^+$	954	0.0023		38	64
$3_6^+ \to 2_6^+$		0.4183	0.00004		3.6
$\to 4_1^+$		0.0022	0.0000		5.4
$\to 2_1^+$	985	0.0040	0.0000	100	90.9
$4_6^+ \to 3_6^+$		0.3084	0.00006		1
$\to 6_1^+$		0.0006			0.1
$\to 2_6^+$		0.1392			23
$\to 4_1^+$	818	0.0043	0.00002	100	32
$\to 2_1^+$		0.0010			44
$7_2^- \to 5_3^-$		0.0469			0.9
$\to 5_2^-$	318	0.2132		100	99
$9_2^- \to 7_3^-$		0.0251			0.2
$\to 7_2^-$	430	0.2926		100	100
$11_2^- \to 9_3^-$		0.0040			0.1
$\to 9_2^-$	519	0.3296		100	100
$13_2^- \to 11_2^-$	605	0.3240		100	100
$15_2^- \to 13_2^-$	689	0.2988		100	100
$17_2^- \to 15_2^-$	767	0.2600		100	100
$19_2^- \to 17_2^-$	834	0.2113		100	100
$5_3^- \to 5_2^-$	150	0.0001	0.0058	28	37
$\to 4_3^-$	155	0.1175	0.0069	72	63
$6_3^- \to 5_3^-$	178	0.0866	0.0148	40	6
$\to 5_2^-$	327	0.0087	0.0176	25	43
$\to 4_3^-$	332	0.2679		35	51
$7_3^- \to 6_3^-$	223	0.0767	0.0026	41	2
$\to 7_2^-$	232	0.0019	0.0010	8	0.5
$\to 5_3^-$	401	0.2684		51	57
$\to 5_2^-$		0.0386			40.5
$8_3^- \to 7_3^-$	226	0.0711	0.0274	25	4
$\to 6_3^-$	450	0.3134		75	54
$\to 7_2^-$		0.0052	0.0311		42
$9_3^- \to 8_3^-$	291	0.0616	0.0121	30	3.6
$\to 9_2^-$		0.0015	0.0012		0.4
$\to 7_3^-$	517	0.3139		70	71
$\to 7_2^-$		0.0169			25
$10_3^- \to 9_3^-$		0.0567	0.0351		3
$\to 8_3^-$	542	0.3412		100	58
$\to 9_2^-$		0.0013	0.0395		39
$12_3^- \to 10_3^-$	637	0.3421		100	64
$\to 11_2^-$		0.0007	0.0427		36
$7_4^- \to 6_4^-$	200	0.2189	0.0683	45	35
$8_4^- \to 7_4^-$	229	0.3001	0.0144	45	35
$\to 6_4^-$	429	0.0245		< 10	30
$9_4^- \to 8_4^-$	254	0.3766	0.0013	58	22
$\to 7_4^-$	483	0.0592		42	78
$10_4^- \to 9_4^-$	260	0.3843	0.0235	27	22
$\to 8_4^-$	513	0.1008		73	78
$11_4^- \to 10_4^-$	295	0.3620	0.0609	38	29
$\to 9_4^-$	555	0.1404		62	71
$12_4^- \to 11_4^-$	323	0.3281	0.0960	30	27
$\to 10_4^-$	619	0.1715		70	73
$13_4^- \to 12_4^-$	344	0.2893	0.1415	84	27
$\to 11_4^-$	667	0.1995		< 16	73
$14_4^- \to 13_4^-$		0.2574	0.1675		26
$\to 12_4^-$	714	0.2159		100	74
$16_4^- \to 14_4^-$	800	0.2363		100	100

References

1. C. Rossi Alvarez, Nucl. Phys. News **3**, no. 3 (1993).
2. K.L Ying *et al.*, J. Phys. G **12**, L211 (1986).
3. J. Lu *et al.*, Nucl. Phys. A **608**, 327 (1996).
4. T. Morek, K. Starosta, Ch. Droste, D. Fossan, G. Lane, J. Sears, J. Smith, P. Vaska, Eur. Phys. J. A **3**, 99 (1998).
5. A.N. Wilson *et al.*, Phys. Rev. C **63**, 054307 (2001).
6. E. Farnea, G. de Angelis, D. De Acuna, A. Gadea, D.R. Napoli, P. Spolaore, A. Buscemi, R. Zanon, R. Isocrate, D. Bazzacco, C. Rossi Alvarez, P. Pavan, A.M. Bizzetti-Sona, P.G. Bizzetti, Nucl. Instrum. Methods Phys. Res. A **400**, 87 (1997).
7. C.M. Petrache, D. Bazzacco, S. Lunardi, C. Rossi Alvarez, G. de Angelis, M. De Poli, D. Bucurescu, C.A. Ur, P.B. Semmes, R. Wyss, Nucl. Phys. A **597**, 106 (1996).
8. E.S. Paul *et al.*, Nucl. Phys. A **676**, 32 (2000).
9. F. Iachello, D. Vretenar, Phys. Rev. C **43**, 945 (1991).
10. D. Vretenar, G. Bonsignori, M. Savoia, Phys. Rev. C **47**, 2019 (1993).
11. D. Vretenar, G. Bonsignori, M. Savoia, Z. Phys. A **351**, 289 (1995).
12. D. Vretenar, S. Brant, G. Bonsignori, L. Corradini, C.M. Petrache, Phys. Rev. C **57**, 675 (1998).
13. A. Arima, F. Iachello, Phys. Rev. Lett. **35**, 1069 (1975).
14. F. Iachello, A. Arima, *The Interacting Boson Model* (Cambridge University Press, Cambridge, 1987).
15. F. Iachello, P. Van Isacker, *The Interacting Boson-Fermion Model* (Cambridge University Press, Cambridge, 1991).
16. A. Osa, M. Asai, M. Koizumi, T. Sekine, S. Ichikawa, Y. Kojima, H. Yamamoto, K. Kawade, Nucl. Phys. A **588**, 185c (1995).
17. C.M. Petrache, M. Nespolo, S. Brant, G. Lo Bianco, D. Bazzacco, S. Lunardi, P. Spolaore, M. Axiotis, N. Blasi, G. de Angelis, T. Kröll, N. Marginean, T. Martinez, R. Menegazzo, D.R. Napoli, B. Quintana, A. Saltarelli, A. Ventura, D. Vretenar, Phys. Rev. C **64**, 044303 (2001).
18. L.S. Kisslinger, R.A. Sorensen, Rev. Mod. Phys. **35**, 853 (1963).
19. Gh. Cata-Danil, D. Bucurescu, A. Gizon, J. Gizon, J. Phys. G **20**, 1051 (1994).
20. C.M. Petrache *et al.*, Eur. Phys. J. A **14**, 439 (2002).
21. C.M. Petrache, R. Venturelli, D. Vretenar, D. Bazzacco, G. Bonsignori, S. Brant, S. Lunardi, N.H. Medina, M.A. Rizzutto, C. Rossi Alvarez, G. de Angelis, M. De Poli, D.R. Napoli, Nucl. Phys. A **617**, 228 (1997).
22. R. Wyss, A. Grandearth, R. Bengtsson, P. von Brentano, A. Dewald, A. Gelberg, A. Gizon, J. Gizon, S. Harissopulos, A. Johnson, W. Lieberz, W. Nazarewicz, J. Nyberg, K. Schiffer, Nucl. Phys. A **505**, 337 (1989).